



http://pubs.acs.org/journal/acsodf Article

Probing Electronic Communication and Excited-State Dynamics in the Unprecedented Ferrocene-Containing Zinc MB-DIPY

Yuriy V. Zatsikha, Liliya I. Shamova, Jacob W. Schaffner, Andrew T. Healy, Tanner S. Blesener, Gabriel Cohen, Brandon Wozniak, David A. Blank,* and Victor N. Nemykin*



Cite This: ACS Omega 2020, 5, 28656–28662



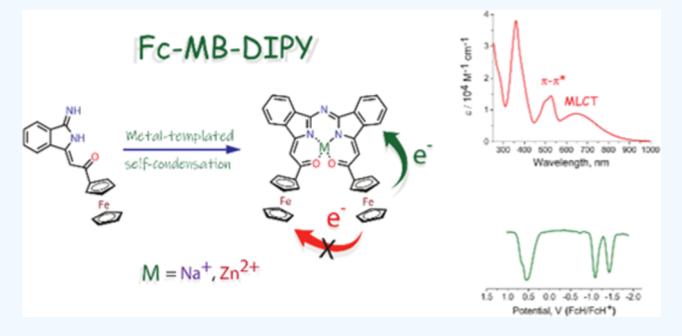
ACCESS I

Metrics & More

Article Recommendations

3 Supporting Information

ABSTRACT: The electronic communication between two ferrocene groups in the electron-deficient expanded aza-BODIPY analogue of zinc manitoba-dipyrromethene (MB-DIPY) was probed by spectroscopic, electrochemical, spectroelectrochemical, and theoretical methods. The excited-state dynamics involved subps formation of the charge-separated state in the organometallic zinc MB-DIPYs, followed by recovery of the ground state via charge recombination in 12 ps. The excited-state behavior was contrasted with that observed in the parent complex that lacked the ferrocene electron donors and has a much longer excited-state lifetime (670 ps for the singlet state). Much longer decay times observed for the parent complex without ferrocene confirm that the



main quenching mechanism in the ferrocene-containing 4 is reflective of the ultrafast ferrocene-to-MB-DIPY core charge transfer (CT).

■ INTRODUCTION

The chemistry of functional dyes connected to redox-active fragments, and in particular to ferrocene groups, has gained significant interest because of their potential use in photocatalysis, molecular electronics, redox-switchable fluorescence, and light-harvesting applications. 1,2 Electronic communication between the ferrocene groups and the excited-state dynamics (in particular the formation and lifetime of charge-separated states) in ferrocene-containing porphyrins, 3,4 phthalocyanines, 5,6 BODIPYs, 7,9 aza-BODIPYs, 10,11 and BOPHYs 12 were probed by a variety of spectroscopic, electrochemical, and theoretical methods. Because of their excellent photophysical properties, the use of the electron-deficient BODIPY analogues is attractive for solar light-harvesting applications. BODIPYs with electron-accepting groups in meso- $^{13-15}$ or β position(s), 16-18 pyridone-conjugated BODIPYs, 19-24 and aza-BODIPYs²⁵⁻²⁹ have comparable first reduction potentials to C₆₀ fullerene derivatives and have demonstrated significantly better optical and photophysical properties for light harvesting. Despite such a prominent and potentially useful combination of redox and optical properties, studies on ferrocenecontaining systems connected to the electron-deficient chromophore are sparse. 30-34 We have recently developed a scalable synthetic pathway for the preparation of the electrondeficient manitoba-dipyrromethene (MB-DIPY) chromophores that are direct analogues of the benzo-fused aza-DIPYs and aza-BODIPYs.³⁵ In this communication, we will show that the readily available and inexpensive acetylferrocene

can be used as a precursor for the preparation of the first ferrocene-containing MB-DIPY analogues with similar absorption and redox properties to C_{60} fullerene and its derivatives.

■ RESULTS AND DISCUSSION

Synthesis of the unprecedented ferrocene-containing MB-DIPYs is shown in Scheme 1 with all synthetic and characterization data provided in the Experimental Section and Supporting Information Figures S1–S11. It follows the procedure previously developed by our group³⁵ that uses acetylferrocene 1 as a precursor for the formation of 2. This precursor was then used for the formation of sodium MB-DIPYs 3 in good yield. The final zinc MB-DIPY complex 4 was prepared by transmetalation of the sodium salts 3 with the zinc acetate in tetrahydrofuran (THF). Reduction products of 4 ([4]• and [5] were prepared by the chemical reduction with NaBH₄ or under spectroelectrochemical conditions to gain spectroscopic features of the reduced MB-DIPY core. Because of their low stability in solution, these materials were not isolated or fully characterized.

Received: August 5, 2020 Accepted: October 15, 2020 Published: October 27, 2020





Scheme 1. Synthesis of Ferrocene-Containing MB-DIPYs 3, 4^{\bullet} and Their One- and Two-Electron Reduced Derivatives $[4]^{\bullet}$ and $[5]^{-a}$

Fc
$$=$$
 Fe $=$ Fc $=$ F

"Reagents and conditions: (i) NaH, DMF, 1,2-dicyanobenzene, r.t., 10 h; (ii) NaH, 1,4-dioxane, reflux, 3 h; (iii) Zn(OAc)₂ 2H₂O, THF, r.t., 30 min; (iv) NaBH₄, THF, r.t.; and (v) 25% NMe₄OH in MeOH, r.t.

The UV-vis spectra of the sodium and zinc derivatives 3 and 4 are presented in Figure 1. Zinc complex 4 has a similar

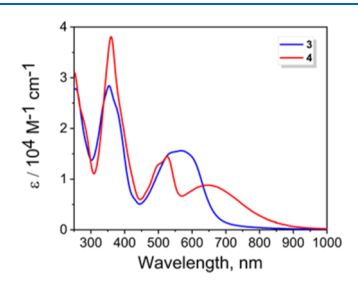


Figure 1. UV-vis absorption spectra of MB-DIPYs 3 (THF) and 4 (DCM).

absorption profile to the ferrocene-BODIPYs and ferrocene-aza-BODIPYs $^{7-11}$ with MB-DIPY centered $\pi-\pi^*$ transitions observed at $\sim\!500$ nm and a lower-intensity, lower-energy broad metal-to-ligand charge-transfer (MLCT) band observed at $\sim\!670$ nm (Supporting Information Figure S13). The MLCT band in 3 overlaps with the MB-DIPY-centered $\pi-\pi^*$ transitions forming a broad absorption envelope between 500 and 600 nm. Thus, unlike the previously reported zinc MB-DIPYs with the other terminal aryl substituents, the UV-vis spectra of the ferrocene-containing MB-DIPYs 3 and 4 have additional MLCT bands with lower energies compared to the ligand-centered $\pi-\pi^*$ transitions in agreement with their electronic structure calculations discussed below.

The redox properties of the new donor—acceptor dyad 4 were probed by electrochemical and spectroelectrochemical methods (Figures 2, 3, and S12). Cyclic voltammetry (CV) and differential pulse voltammetry (DPV) experiments identified one two-electron oxidation and two single-electron reduction processes in DCM/0.1 M TBAP (Figure 2). In low ion-pairing DCM/0.05 M TFAB (TFAB = tetrabutylammonium tetrakis[pentafluorophenyl] borate), the first two, closely spaced, oxidation processes were measured (Supporting Information Figure S12). In both systems, the shape of the cathodic and anodic waves for the oxidation was characteristic of an adsorption/desorption process at the working electrode. So Based on the ferrocene-BODIPY and ferro-

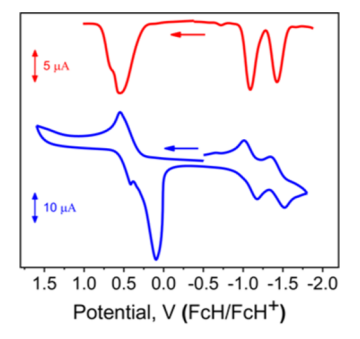


Figure 2. DPV (top) and CV (bottom) data on MB-DIPY 4 in 0.1 M TBAP in the DCM system.

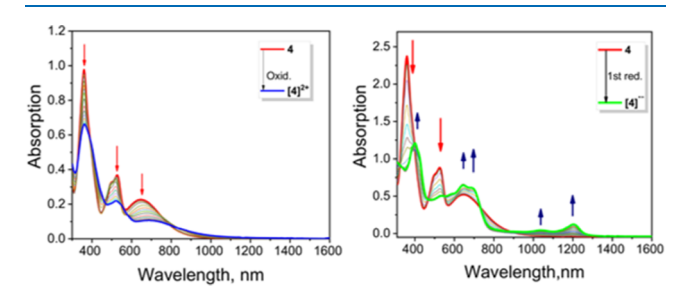


Figure 3. UV—vis—NIR absorption spectra of MB-DIPY 4 (red) and its two-electron-oxidized [4]²⁺ (blue) and one-electron reduced [4]^{•–} (green) derivatives obtained under spectroelectrochemical oxidation/reduction conditions in the deoxygenated 0.3 M TBAP/DCM system. The discontinuity at 850 nm reflects a detector change.

cene-aza-BODIPY⁵ data, the first oxidation process was assigned to a ferrocene-centered oxidation. The oxidation potentials in 4 are close to that in acetylferrocene (Supporting Information Table S1).

Based on the previous data for MB-DIPYs, 35 we have assigned both reduction processes to the reduction of the MB-DIPY chromophore. The first reduction in 4 occurs at a potential close to that observed for the first reduction potential of C_{60} fullerene and its derivatives. 36,37 Derivative 3 was too moisture sensitive to conduct electrochemical and spectroelectrochemical experiments without being hydrolyzed to the

metal-free MB-DIPY. Unlike ferrocene-BODIPYs, $^{7-9}$ ferrocene-aza-BODIPYs, 10,11 and ferrocene-BOPHYs, 12 oxidation of 4 under spectroelectrochemical or chemical oxidation conditions did not show evidence of the characteristic intervalence charge transfer (IVCT) band in the near-infrared (NIR) region. 10,11 Similar behaviors were observed in the case of several conformationally flexible ferrocene-pyridoneBODI-PYs²¹ and ferrocene-BOPHYs.³⁸ However, zinc complex 4 is conformationally rigid, and thus, the absence of the IVCT band during oxidation is indicative of a lack of electronic communication between two ferrocene groups. Taking into consideration that the density functional theory (DFT)predicted Fe-Fe distance in 4 is comparable to or shorter than the Fe-Fe distances in the ferrocene-BODIPYs^{7,9} and ferrocene-BOPHYs, 12 in which electronic coupling between two iron centers was observed, we speculate that lack of longrange metal-metal coupling in 4 might be attributed to either the inverted electronic structure of MB-DIPY compared to the traditional BODIPYs and aza-BODIPYs, with the highestoccupied molecular orbital (HOMO) located on the ferrocene rather than the core, or interruption of the electronic coupling in 4 by sp²-hybridized carbonyl C=O groups. The singleelectron reduction of zinc complex 4 under spectroelectrochemical or chemical reduction conditions (Figures 3 and 4) is

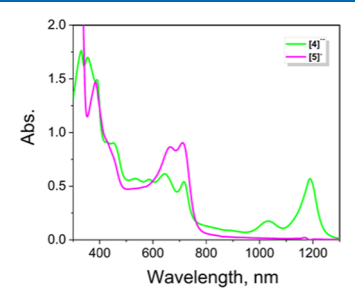


Figure 4. UV-vis-NIR absorption spectra of one-electron-reduced [4]*- (green) and two-electron-reduced [5]- (magenta) zinc MB-DIPY derivatives obtained by the reduction with NaBH₄ in THF.

similar to that observed earlier for MB-DIPYs.³⁵ Formation of the low-energy bands at 1190 and 1034 nm is indicative of the reduction of the MB-DIPY core. This anion radical was not stable and can be easily reoxidized to the initial 4 under spectroelectrochemical conditions or by simple exposure of [4]^{•–} to air. The second reduction of 4 can be achieved in the NaBH₄/NMe₄OH system. Similar to other zinc MB-DIPYs,³⁴ during the second reduction, both NIR bands disappeared and two new intense bands at 711 and 665 nm appear in the spectrum of [5][–] (Figure 4).

Excited-state dynamics for 4 were measured using pump-probe spectroscopy (Figures 5, S22–S24). Following excitation at 400 nm, transient absorption, TA, was evident at wavelengths shorter than 525 nm and throughout the near-IR. In the first picosecond after excitation, the TA shifted spectrally, to shorter wavelengths in the visible and longer wavelengths in the near IR, and decreased in intensity. Subsequently, there was a bimodal reduction in intensity on time scales of tens and hundreds of picoseconds. To quantify the time scales, the data at individual probe wavelengths were fitted as a series of first-order kinetic events. The fitting function and optimized fitting parameters are presented in the Supporting Information, and the fits are shown in the bottom panel of Figure 5. Using the 950 nm probe as an example, the

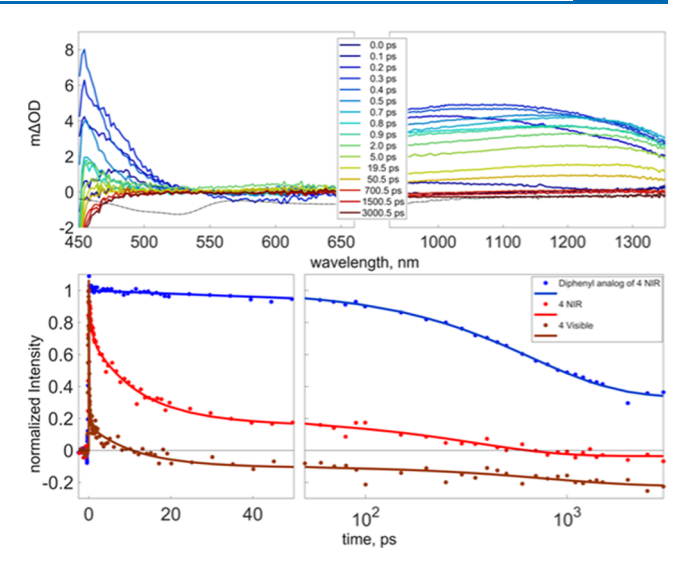


Figure 5. Transient change in optical density following excitation of 4 in DCM at 400 nm. The dashed line in the upper two panels represents the inverted absorption spectrum for reference. In the bottom panel, the circles are the time evolution of the dominant principle component of the singular value decomposition (SVD) analysis and the solid lines are the fit to a sequential set of first-order events (Supporting Information Figures S22–S24).

three sequential time scales are 0.27 \pm 0.03, 12 \pm 2, and 300 \pm 0.03 ps.

Excitation at 400 nm was predominantly a $\pi \to \pi^*$ transition of the MB-DIPY core; 39 the HOMO $-4 \rightarrow$ lowest unoccupied molecular orbital (LUMO) + 1 transition in 4 was based on the time-dependent DFT (TDDFT) results below. The transient absorption was analyzed using singular value decomposition (SVD). In all cases, time evolution of the dominate principle component was fitted to characterize the time constants associated with a change in the TA (Supporting Information and Table S2). The resulting fits are presented in Figure 5. In the absence of the Fc electron donors, the π^* excited state demonstrates broad transient absorption across the visible and NIR with the fastest decay time constant of 670 ± 60 ps, see the bottom of Figure 5 and Supporting Information. However, when Fc groups were added, 4, there was a rapid loss of TA in the first picosecond after excitation in the visible and NIR with an initial sub-picosecond time constant (130 \pm 6 fs in the visible) followed by a 12 \pm 2 ps loss of TA. The fastest component is assigned to an initial charge transfer event from the Fc to the singly occupied π orbital to create the charge transfer (CT) state. At this point, NIR absorption remains due to TA from the electron in the excited π^* orbital. The 12 ps time constant follows loss of the CT state and return to the ground electronic state through the transfer of the electron in the π^* orbital to the singly occupied HOMO centered on the Fc. The energetic driving force for the initial charge separation and subsequent charge recombination are illustrated in Figure 6. These dynamics, ultrafast transfer of an electron from the HOMO on the donor to the π orbital on the core opened by the initial excitation, followed by subsequent charge recombination via transfer from the excited π^* to the HOMO, are analogous to excited-state deactivation in catechol-containing BODIPYs, aza-BODIPYs, and BO-PHYs. 40 The longest time scale measured was small in amplitude, poorly determined, and varied somewhat depending on the probe wavelength. This may represent some degree

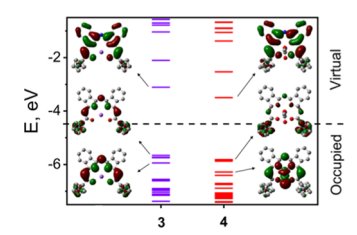


Figure 6. MO energies of MB-DIPYs 3 (left) and 4 (right) predicted by DFT calculations along with their frontier orbital images.

of thermalization following charge recombination back to the ground state.

To gain additional insight into the spectroscopic and redox properties of the sodium and zinc complexes, 3 and 4, density functional theory (DFT) and time-dependent DFT (TDDFT) calculations were performed on these systems. The DFT-predicted energy level diagram is shown in Figure 6, and the frontier MO compositions for 3 and 4 are listed in Supporting Information Figures S14–S17.

In good agreement with the experimental electro- and spectroelectrochemical data, the HOMO in all compounds was predicted to be dominated by contributions from the two ferrocene fragments, while the LUMO is MB-DIPY centered. The LUMO in complexes 3 and 4 resembled the HOMO in typical BODIPYs and aza-BODIPYs, with the large contributions coming from orbitals on the nitrogen atoms. The highest energy occupied MO that has a predominant MB-DIPY character was the HOMO-4 in 3 and 4. In agreement with our earlier calculations, his MO resembled the typical LUMO in regular BODIPYs and aza-BODIPYs and was dominated by contributions from the α - and β -carbon atoms of isoindole fragments. The spin density in [4]• was predominantly localized on the MB-DIPY core (Supporting Information Figure S18), while the HOMO of the two-electron reduced [5] resembled that of a typical BODIPY.

TDDFT calculations on 3, 4, and [4]•-, [5]- (Figure 7 and Supporting Information Figures S18–S21) were in agreement

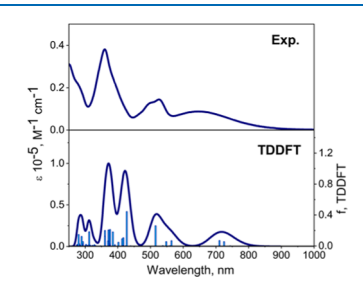


Figure 7. Experimental (top) and TDDFT-predicted (bottom) UV—vis—NIR spectra of zinc MB-DIPY 4 in DCM.

with the experimental UV-vis spectra. Similar to the previously reported ferrocene-BODIPYs⁴ and ferrocene-aza-BODIPYs, ^{10,11} TDDFT predicts several predominantly MLCT transitions that have energies lower than the most intense, MB-DIPY-centered $\pi-\pi^*$ band (see Supporting Information for the detailed analysis). The energy difference between a cluster of MLCT bands and the low-energy $\pi-\pi^*$ in 3 (Supporting Information Figure S19) was significantly smaller than it is in 4 (Figure 7). This correlated well with the experimental observations. TDDFT calculations on single-electron reduced [4]• were consistent with the two experimentally measured

NIR bands. These bands were predicted to disappear upon a second reduction to [5], in agreement with the experiment (Supporting Information Figures S20 and S21).

CONCLUSIONS

In conclusion, we have prepared and characterized sodium and zinc derivatives of the first ferrocene-containing MB-DIPY compounds, where the ferrocene groups are conjugated to the benzo-fused aza-BODIPY core. Despite a ferrocene-dominated HOMO and modest Fe-Fe distance in 4, the electrochemical and spectroelectrochemical experiments indicated very little, if any, electronic coupling between the two iron centers. The first reduction potential in complex 4 was close to that observed in C₆₀ fullerene and its derivatives. The reduction of 4 led to the formation of the anion-radical [4]*-, which absorbs strongly in the NIR region. The time-resolved spectroscopy confirmed the ultrafast initial formation of the charge-separated state in complexes 4, which subsequently decayed in 12 ps to the ground state. The low-lying CT state provided efficient deactivation of the initial π^* excited state, with the lifetime reduced by a factor of 20 compared with MB-DIPYs that lack the ferrocene groups. The charge recombination excited-state deactivation was also faster than previously reported in the analogous ferrocene-BODIPYs.

EXPERIMENTAL SECTION

Materials. Solvents were purified using standard approaches: THF and 1,4-dioxane were dried over sodium metal and benzophenone, and DCM was dried over phosphorous(V) oxide. Phthalonitrile, sodium hydride, sodium borohydride, zinc acetate dihydrate, and 25% methanolic solution of tetramethylammonium hydroxide were purchased from Sigma Aldrich. All air-sensitive reactions were carried out under dry argon atmosphere using Schlenk-tube and vacuum-line techniques.

Spectroscopy Measurements. A Jasco-V770 spectrophotometer was used to collect UV-vis data. Standard rectangular 1 × 1 cm quartz cuvettes were used for all of the measurements. Spectra shown in Figures 1, 2, and 7 are measured in DCM at ambient conditions (as indicated in the figure captures). Spectra shown in Figure 4 are measured in THF at ambient conditions (as indicated in the figure capture). NMR spectra were recorded on a Bruker Avance instrument with a 300 MHz frequency for protons and 75 MHz frequency for carbons. Chemical shifts are reported in parts per million (ppm) and referenced to the residual proton resonance of the deuterated solvent (CDCl₃ = δ 7.26; THF- d_8 = δ 1.73), and carbon spectra are referenced to the carbon resonances of the solvent (CDCl₃ = δ 77.16; THF- d_8 = δ 25.37). High-resolution mass spectra of all new compounds were recorded using a Bruker micrOTOF-QIII. All exact mass measurements showed an error of less than 5 ppm.

Electrochemistry and Spectroelectrochemistry. Electrochemical cyclic voltammetry (CV) and differential pulse voltammetry (DPV) measurements were conducted using a CHI-620 C electrochemical analyzer utilizing a three-electrode scheme with platinum working, auxiliary, and Ag/AgCl reference electrodes. The typical scan rate for CV experiment was 100 mV/s. DCM was used as a solvent, and 0.1 M solution of tetrabutylammonium perchlorate (TBAP) and 0.05 M tetrabutylammonium terakis(pentafluorophenyl)borate (TFAB) were used as supporting electrolytes. Spectroelec-

trochemical experiments were conducted in DCM/0.3 M TBAP system using a custom-made 1 mm cell and platinum mesh working electrode. The typical time for spectroelectrochemical experiments varies between 40 and 120 min. In all cases, experimental redox potentials were corrected using decamethylferrocene (Fc*H) as an internal standard.

Computational Details. The starting geometries of MB-DIPYs 3, 4, [4]•-, and [5]- were optimized using a hybrid B3LYP exchange—correlation functional.⁴¹ Frequencies were calculated to ensure the stationary geometry. Solvent effects were calculated using the polarized continuum model (PCM).⁴² In all calculations, DCM was used as the solvent. In PCM-TDDFT calculation, the first 50 states were calculated in the case of compounds 3 and 4, 100 states were calculated for compound [4]•-, and 80 states were calculated for compound [5]-. Full-electron Wachter's basis set⁴³ was utilized for iron atoms, while all other atoms were modeled using 6-311G(d)⁴⁴ basis set. Gaussian 09 software was used in all calculations.⁴⁵ QMForge program was used for molecular orbital analysis.⁴⁶

Pump-Probe Experimental Setup. A home-built, regeneratively amplified Ti:sapphire laser system produced ~80 fs, 1 mJ, 810 nm pulses at a repetition of 1 kHz. A 90% portion of this output was frequency doubled by a 1 mm BBO crystal to produce 400 nm excitation pump pulses. The remaining 10% of the output was focused into a 2 mm sapphire plate (visible) or 2 mm YAG (Yttrium Aluminum Garnet) plate (NIR) to create the continuum probe pulses. Pump pulses were modulated at half the repetition rate of the laser by a mechanical chopper. The pump was polarized at 54.7° relative to the probe to minimize the influence of anisotropic dynamics on the measurements. The time delay between the pump and probe pulses was controlled by a mechanically delayed stage. The pump and probe beams were focused and crossed in a 1 mm path length sample quartz cuvette. The pump energy was 1 μ J per pulse with a spot size of 164 μ m (1/ e²) for the visible pump-probe studies and spot size of 214 μ m (1/e²) for near-infrared (NIR) studies. Samples were dissolved in dichloromethane, purged with argon for 5 min prior to each measurement, and flowed throughout the entire experiment using a peristaltic pump. The visible probe beam was collimated after the sample, focused into a monochromator (Princeton Instruments SP2150i monochromator 150 lines/mm, 500 nm blaze), and detected on a 256-pixel linear diode array (Hamamatsu S3902-256Q). For experiments detecting in the NIR, detection was done using a Princeton Instruments SP2150 monochromator (150 lines/mm, 1200 nm blaze) with a 256 linear InGaAs diode array (Hamamatsu G9213-256S). Measuring the probe beam with and without the pump for each sequential pair of laser pulses provided the change in optical density, ΔOD , on a shot to shot basis. The spectra presented represent the average of 30 000 pulse pairs at each time delay. The samples had an optical density of 0.25-0.30 at the pump wavelength. Absorption spectra were taken before and after pump-probe data collection, and no change was observed within experimental error, suggesting a lack of photodegradation during the experiments.

Pump—Probe SVD Analysis. Figures S22—S24 present the SVD analysis of the pump—probe results for the diphenyl analog of 4 and 4 excited at 400 nm. The SVD analysis was done using publicly available software package Glotaran (http://glotaran.org/). Time constants were determined for the change in amplitude of the dominant principle component.

Time constants are presented in Table S2. Figures present the first four SVD principle components, and the amplitudes for the first 20 components.

Synthetic Procedures. 2-[(1Z)-3-imino-2,3-dihydro-1Hisoindol-1-ylidene]-1-ferrocenylethane-1-one (2). The solution of acetylferrocene 1 930 mg (4.07 mmol) in dry DMF (50 mL) was treated with solid sodium hydride (8.15 mmol, 200 mg) at 0 °C under argon atmosphere. The resulting mixture was stirred for 5 min at 0 °C. Then, the solution of phthalonitrile (4.88 mmol, 625 mg) in dry DMF (20 mL) was slowly added. The resulting solution was stirred for another 5 min at 0 °C and then at room temperature overnight. Then, deep purple solution formed, which was quenched with water (20 mL), neutralized with aqueous ammonium chloride solution and stirred for another 30 min. Then, the resulting deeply colored purple precipitate was collected by vacuum filtration, washed with water, and air-dried to give 1340 mg (92%) of pure compound 2 as a deep purple solid. ${}^{1}H$ NMR (300 MHz, CDCl₃) δ 11.02 (br.s, 1H), 8.18– 8.15 (m, 2H), 8.02-7.96 (m, 2H), 6.61 (s, 1H), and 5.26 (t, $J_{HH} = 3.0 \text{ Hz}, 2\text{H}$; 4.92 (t, $J_{HH} = 3.0 \text{ Hz}, 2\text{H}$); 4.58 (s, 5H); ¹³C NMR (75 MHz, CDCl₃) δ 148.9, 136.7, 131.4, 131.2, 121.2, 92.3, 81.5, 72.8, 70.2, and 69.4; HRMS (APCI-TOF) m/z: [M - H]⁻ Calcd for C₂₀H₁₆N₂OFe 355.0528; found 355.0576.

Compound **3**. The solution of compound 3 (300 mg, 0.84 mmol) was treated with sodium hydride powder (14 mg, 0.50 mmol) in dry 1,4-dioxane (20 mL) under argon atmosphere. The resulting mixture was stirred for 5 min at room temperature, then under refluxed conditions for 3 h. Then, the solution was cooled down to room temperature, diluted with dry hexane (100 mL), and left for 3 h for crystallization. The resulting precipitate was collected by vacuum filtration and air-dried to give 259 mg (86%) of pure compound **3**. ¹H NMR (300 MHz, THF- d_8) δ 8.04–8.01 (m, 2H), 7.96–7.93 (m, 2H), 7.51–7.43 (m, 4H), 6.79 (s, 2H), 5.10 (s, 4H), 4.60 (s, 4H), and 4.25 (s, 10H); ¹³C NMR (75 MHz, THF- d_8) δ 194.7, 175.7, 162.1, 143.7, 142.4, 129.9, 129.6, 122.9, 120.5, 104.0, 84.8, 73.0, 70.8, and 70.6; HRMS (APCI-TOF) m/z: [M]⁻ Calcd for $C_{40}H_{28}N_3Fe_2O_2Na$ 717.0774; found 717.0808.

Compound 4. To the solution of compound 3 (100 mg, 0.14 mmol) in THF (15 mL), the suspension of zinc(II) acetate dihydrate (34 mg, 0.15 mmol) in THF (4 mL) was added. The resulting mixture was stirred for 4 h at room temperature. Then, the resulting precipitate was collected by filtration, and the crude product was additionally dried in a high vacuum for 1 h to give 70 mg (60%) of pure zinc complex 4. 1 H NMR (300 MHz, CDCl₃) δ 8.16–8.14 (m, 2H), 7.88– 7.86 (m, 2H), 7.63-7.55 (m, 4H), 6.71 (s, 2H), 5.32-5.25 (m, 2H), 5.06-5.02 (m, 2H), 4.86-4.76 (m, 4H), 4.38 (s, 10H), 3.77-3.73 (m, 4H), and 1.87-1.83 (m, 4H), 1.80 (s, 3H); 13 C NMR (75 MHz, CDCl₃) δ 197.2, 175.0, 158.6, 140.1, 138.5, 130.9, 130.8, 123.7, 120.9, 103.4, 82.2, 74.3, 74.1, 71.3, 70.8, 70.5, 68.1, 25.7, and 23.9; HRMS (APCI-TOF) m/ z: $[M - OAc]^+$ Calcd for $C_{40}H_{28}N_3Fe_2O_2Zn$ 758.0169; found 758.0266.

Compounds [4]^{•-} and [5]⁻. The suspension of zinc(II) complex 4 (41 mg, 0.05 mmol) in dry THF (10 mL) was treated with sodium borohydride (6 mg, 0.15 mmol) under argon atmosphere. The resulting mixture was stirred for 10 min yielding [4]^{•-} as a deep green solution. Then, the solution was treated with 25% methanolic tetramethylammonium hydroxide solution (18 mg, 0.05 mmol) and stirred for

another 5 min yielding a green solution of two-electron reduced anionic zinc(II) complex [5]. Due to the low stability of the obtained dyes, they were immediately subjected to UV—vis absorption spectroscopy analyses.

Compound [4]•-. UV/vis (THF): $\lambda_{\text{max}} = 1190$, 1034, 716, 644, 585, 535, 450, and 390 nm.

Compound [5]⁻. UV/vis (THF): $\lambda_{\text{max}} = 711$, 665, and 390

ASSOCIATED CONTENT

Solution Supporting Information

The Supporting Information is available free of charge at https://pubs.acs.org/doi/10.1021/acsomega.0c03764.

Experimental and theoretical characterization data for compounds 3 and 4 as well as starting materials and reference compounds (PDF)

AUTHOR INFORMATION

Corresponding Authors

David A. Blank – Department of Chemistry, University of Minnesota, Minneapolis, Minnesota 55455, United States; orcid.org/0000-0003-2582-1537; Email: blank@umn.edu

Victor N. Nemykin — Department of Chemistry, University of Manitoba, Winnipeg, Manitoba R3T 2N2, Canada; Department of Chemistry, University of Tennessee, Knoxville, Tennessee 37996, United States; Occid.org/0000-0003-4345-0848; Email: vnemykin@utk.edu

Authors

Yuriy V. Zatsikha — Department of Chemistry, University of Manitoba, Winnipeg, Manitoba R3T 2N2, Canada; orcid.org/0000-0002-9770-7007

Liliya I. Shamova – Department of Chemistry, University of Manitoba, Winnipeg, Manitoba R3T 2N2, Canada

Jacob W. Schaffner – Department of Chemistry, University of Minnesota, Minneapolis, Minnesota 55455, United States; orcid.org/0000-0003-4970-3789

Andrew T. Healy – Department of Chemistry, University of Minnesota, Minneapolis, Minnesota 55455, United States

Tanner S. Blesener – Department of Chemistry, University of Manitoba, Winnipeg, Manitoba R3T 2N2, Canada

Gabriel Cohen – Department of Chemistry, University of Manitoba, Winnipeg, Manitoba R3T 2N2, Canada

Brandon Wozniak – Department of Chemistry, University of Manitoba, Winnipeg, Manitoba R3T 2N2, Canada

Complete contact information is available at: https://pubs.acs.org/10.1021/acsomega.0c03764

Notes

The authors declare no competing financial interest.

ACKNOWLEDGMENTS

Generous support from the Minnesota Supercomputing Institute, NSERC, CFI, University of Manitoba, and WestGrid Canada to V.N.N. is greatly appreciated. Generous support from the NSF support (DMR-1708177) to D.A.B. is also greatly appreciated.

ABBREVIATION

MB-DIPY(or manitoba-dipyrromethene) is the common name of the ligand. The preferred IUPAC names for compounds 3 and 4 are: 3: 2-[(1Z,3Z)-3-{[(1Z)-1-(2-oxo-2-ferrocenylethy-

lidene)-1H-isoindol-3-yl]imino}-2-sodio-2,3-dihydro-1H-isoindol-1-ylidene]-1-ferrocenylethan-1-one and 4: $[(1Z,3Z)-1-(2-\infty-2-ferrocenylethylidene)-3-{[(1Z)-1-(2-\infty-2-ferrocenylethylidene)-1H-isoindol-3-yl]imino}-2,3-dihydro-1H-isoindol-2-yl]zincio acetate.$

REFERENCES

- (1) Heinze, K.; Lang, H. Ferrocene Beauty and Function. *Organometallics* **2013**, 32, 5623–5625.
- (2) Patra, M.; Gasser, G. The medicinal chemistry of ferrocene and its derivatives. *Nat. Rev. Chem.* **2017**, *1*, No. 0066.
- (3) Pandey, A. K.; Sanfui, S.; Khan, F. S. T.; Rath, S. P. J. Axial ligand mediated switchable rotary motions in a ferrocene-bridged diiron (III) porphyrin dimer. *J. Organomet. Chem.* **2019**, 894, 28–38.
- (4) Mondal, B.; Sen, P.; Rana, A.; Saha, D.; Das, P.; Dey, A. Reduction of CO₂ to CO by an Iron Porphyrin Catalyst in the Presence of Oxygen. *ACS Catal.* **2019**, *9*, 3895–3899.
- (5) Fernandez-Ariza, J.; Krick-Calderon, R. M.; Rodriguez-Morgade, M. S.; Guldi, D. M.; Torres, T. Phthalocyanine—perylenediimide cart wheels. *J. Am. Chem. Soc.* **2016**, *138*, 12963—12974.
- (6) Gonzalez-Cabello, A.; Vazquez, P.; Torres, T. A new phthalocyanine–ferrocene conjugated dyad. *J. Organomet. Chem.* **2001**, 637–639, 751–756.
- (7) Zatsikha, Y. V.; Maligaspe, E.; Purchel, A. A.; Didukh, N. O.; Wang, Y.; Kovtun, Y. P.; Blank, D. A.; Nemykin, V. N. Tuning electronic structure, redox, and photophysical properties in asymmetric NIR-absorbing organometallic BODIPYs. *Inorg. Chem.* **2015**, 54, 7915–7928.
- (8) Hussein, B. A.; Huynh, J. T.; Prieto, P. L.; Barran, C. P.; Arnold, A. E.; Sarycheva, O. V.; Lough, A. J.; Koivisto, B. D. Molecular lemmings: strategies to avoid when designing BODIPY ferrocene dyads for dye-sensitized solar cell applications. *Dalton Trans.* **2018**, 47, 4916–4920.
- (9) Dhokale, B.; Gautam, P.; Mobin, S. M.; Misra, R. Donor–acceptor, ferrocenyl substituted BODIPYs with marvelous supramolecular interactions. *Dalton Trans.* **2013**, *42*, 1512–1518.
- (10) Zatsikha, Y. V.; Holstrom, C. D.; Chanawanno, K.; Osinski, A. J.; Ziegler, C. J.; Nemykin, V. N. Observation of the Strong Electronic Coupling in Near-Infrared-Absorbing Tetraferrocene aza-Dipyrromethene and aza-BODIPY with Direct Ferrocene— α -and Ferrocene— β -Pyrrole Bonds: Toward Molecular Machinery with Four-Bit Information Storage Capacity. *Inorg. Chem.* **2017**, *56*, 991–1000.
- (11) Sharma, R.; Maragani, R.; Misra, R. J. Ferrocenyl aza-dipyrromethene and aza-BODIPY: synthesis and properties. *J. Organomet. Chem.* **2016**, 825–826, 8–14.
- (12) Rhoda, H. M.; Chanawanno, K.; King, A. J.; Zatsikha, Y. V.; Ziegler, C. J.; Nemykin, V. N. Unusually Strong Long-Distance Metal—Metal Coupling in Bis (ferrocene)-Containing BOPHY: An Introduction to Organometallic BOPHYs. *Chem. Eur. J.* **2015**, *21*, 18043—18046.
- (13) Yakubovskyi, V. P.; Didukh, N. O.; Zatsikha, Y. V.; Kovtun, Y. P. A New Approach to the Synthesis of *meso*-CN-Substituted BODIPYs. *ChemistrySelect* **2016**, *1*, 1462–1466.
- (14) Didukh, N. Ó.; Yakubovskyi, V. P.; Zatsikha, Y. V.; Nemykin, V. N.; Kovtun, Y. P. *meso*-Nitromethyl-Substituted BODIPYs—A new type of water switchable fluorogenic dyes useful for further core modifications. *Dyes Pigm.* **2018**, *149*, 774—782.
- (15) Tomilin, D. N.; Sobenina, L. N.; Petrushenko, K. B.; Ushakov, I. A.; Trofimov, B. A. Design of novel *meso*-CF₃-BODIPY dyes with isoxazole substituents. *Dyes Pigm.* **2018**, *152*, 14–18.
- (16) Hohlfeld, B. F.; Gitter, B.; Flanagan, K. J.; Kingsbury, C. J.; Kulak, N.; Senge, M. O.; Wiehe, A. Exploring the relationship between structure and activity in BODIPYs designed for antimicrobial phototherapy. *Org. Biomol. Chem.* **2020**, *18*, 2416–2431.
- (17) Samanta, P. K.; Alam, MdM.; Misra, R.; Pati, S. K. Tuning of hyperpolarizability, and one-and two-photon absorption of donor–acceptor and donor–acceptor–acceptor-type intramolecular charge

- transfer-based sensors. Phys. Chem. Chem. Phys. 2019, 21, 17343–17355.
- (18) LaMaster, D. J.; Kaufman, N. E. M.; Bruner, A. S.; Vicente, M. G. H. Structure Based Modulation of Electron Dynamics in *meso*-(4-Pyridyl)-BODIPYs: A Computational and Synthetic Approach. *J. Phys. Chem. A* **2018**, *122*, 6372–6380.
- (19) Zatsikha, Y. V.; Swedin, R. K.; Healy, A. T.; Goff, P. C.; Didukh, N. O.; Blesener, T. S.; Kayser, M.; Kovtun, Y. P.; Blank, D. A.; Nemykin, V. N. Synthesis, Characterization, and Electron-Transfer Properties of Ferrocene—BODIPY—Fullerene Near-Infrared-Absorbing Triads: Are Catecholopyrrolidine-Linked Fullerenes a Good Architecture to Facilitate Electron-Transfer? *Chem. Eur. J.* 2019, 25, 8401—8414.
- (20) Didukh, N. O.; Yakubovskyi, V. P.; Zatsikha, Y. V.; Rohde, G. T.; Nemykin, V. N.; Kovtun, Y. P. Flexible BODIPY platform that offers an unexpected regioselective heterocyclization reaction toward preparation of 2-pyridone [a]-fused BODIPYs. *J. Org. Chem.* **2019**, *84*, 2133–214.
- (21) Zatsikha, Y. V.; Didukh, N. O.; Blesener, T.; Kayser, M. P.; Kovtun, Y. P.; Blank, D. A.; Nemykin, V. N. Preparation, Characterization, Redox, and Photoinduced Electron-Transfer Properties of the NIR-Absorbing N-Ferrocenyl-2-pyridone BODIPYs. *Eur. J. Inorg. Chem.* **2017**, 2017, 318–324.
- (22) Zatsikha, Y. V.; Yakubovskyi, V. P.; Shandura, M. P.; Kovtun, Y. P. Boradipyrromethenecyanines on the base of a BODIPY nucleus annelated with a pyridone ring: a new approach to long-wavelength dual fluorescent probe design. *RSC Adv.* **2013**, *3*, 24193–24201.
- (23) Zhao, C.; Zhang, J.; Wang, X.; Zhang, Y. Pyridone fused boron-dipyrromethenes: synthesis and properties. *Org. Biomol. Chem.* **2013**, 11, 372–377.
- (24) Khan, T. K.; Rao, M. R.; Ravikanth, M. Synthesis and Photophysical Properties of 3, 5-Bis (oxopyridinyl)-and 3, 5-Bis (pyridinyloxy)-Substituted Boron-Dipyrromethenes. *Eur. J. Org. Chem.* **2010**, 2010, 2314–2323.
- (25) Sauvé, G.; Fernando, R. Beyond fullerenes: designing alternative molecular electron acceptors for solution-processable bulk heterojunction organic photovoltaics. *J. Phys. Chem. Lett.* **2015**, *6*, 3770–3780.
- (26) Sauvé, G. Designing Alternative Non-Fullerene Molecular Electron Acceptors for Solution-Processable Organic Photovoltaics. *Chem. Rec.* **2019**, *19*, 1078–1092.
- (27) Di Scipio, R.; Sauve, G.; Crespo-Hernandez, C. E. Photodynamics in Metal-Chelating Tetraphenylazadipyrromethene Complexes: Implications for Their Potential Use as Photovoltaic Materials. *J. Phys. Chem. C* **2018**, *122*, 13579–13589.
- (28) Zatsikha, Y. V.; Blesener, T. S.; Goff, P. C.; Healy, A. T.; Swedin, R. K.; Herbert, D. E.; Rohde, G. T.; Chanawanno, K.; Ziegler, C. J.; Belosludov, R. V.; Blank, D. A.; Nemykin, V. N. 1, 7-Dipyrene-Containing Aza-BODIPYs: Are Pyrene Groups Effective as Ligands To Promote and Direct Complex Formation with Common Nanocarbon Materials? *J. Phys. Chem. C* 2018, 122, 27893–27916.
- (29) Maligaspe, E.; Pundsack, T. J.; Albert, L. M.; Zatsikha, Y. V.; Solntsev, P. V.; Blank, D. A.; Nemykin, V. N. Synthesis and charge-transfer dynamics in a ferrocene-containing organoboryl aza-BODIPY donor—acceptor triad with boron as the hub. *Inorg. Chem.* **2015**, *54*, 4167–4174.
- (30) Karmakar, M.; Bhatta, S. R.; Giri, S.; Thakur, A. Oxidation-Induced Differentially Selective Turn-On Fluorescence via Photo-induced Electron Transfer Based on a Ferrocene-Appended Coumarin—Quinoline Platform: Application in Cascaded Molecular Logic. *Inorg. Chem.* **2020**, *59*, 4493—4507.
- (31) Wei, J.-N.; Jia, Z.-D.; Zhou, Y.-Q.; Chen, P.-H.; Li, B.; Zhang, N.; Hao, X.-Q.; Xu, Y.; Zhang, B. Synthesis, characterization and antitumor activity of novel ferrocene-coumarin conjugates. *J. Organomet. Chem.* **2019**, *902*, No. 120968.
- (32) Bhatta, S. R.; Bheemireddy, V.; Thakur, A. A Redox-Driven Fluorescence "Off—On" Molecular Switch Based on a 1, 1'-Unsymmetrically Substituted Ferrocenyl Coumarin System: Mimick-

- ing Combinational Logic Operation. Organometallics 2017, 36, 829-838.
- (33) Peng, Y.-D.; Zhou, L.-S.; Chen, L.-L.; Ma, L.; Zhao, Y.; Zhang, W.-W.; Zuo, J.-L. Ferrocene—isocoumarin conjugated molecules: synthesis, structural characterization, electronic properties, and DFT—TDDFT computational study. *Dalton Trans.* **2015**, *44*, 14465—14474.
- (34) Gonzalez, M.; del, C.; Oton, F.; Espinosa, A.; Tarraga, A.; Molina, P. A densely decorated disubstituted ferrocene as an ion-pair recognition receptor. *Chem. Commun.* **2013**, *49*, 9633–9635.
- (35) Zatsikha, Y. V.; Shamova, L. I.; Blesener, T. S.; Kuzmin, I. A.; Germanov, Y. V.; Herbert, D. E.; Nemykin, V. N. Development of a Class of Easily Scalable, Electron-Deficient, Core-Extended Benzo-Fused Azadipyrromethene Derivatives ("MB-DIPY"). *J. Org. Chem.* **2019**, *84*, 14540–14557.
- (36) Xie, Q.; Perez-Cordero, E.; Echegoyen, L. Electrochemical detection of C_{60}^{6-} and C_{70}^{6-} : Enhanced stability of fullerides in solution. *J. Am. Chem. Soc.* **1992**, *114*, 3978–3980.
- (37) Dubois, D.; Kadish, K. M.; Flanagan, S.; Wilson, L. J. Electrochemical detection of fulleronium and highly reduced fulleride (C_{60}^{5-}) ions in solution. *J. Am. Chem. Soc.* **1991**, *113*, 7773–7774.
- (38) Zatsikha, Y. V.; Nemez, D. B.; Davis, R. L.; Singh, S.; Herbert, D. E.; King, A. J.; Ziegler, C. J.; Nemykin, V. N. Testing the Limits of the BOPHY Platform: Preparation, Characterization, and Theoretical Modeling of BOPHYs and Organometallic BOPHYs with Electron-Withdrawing Groups at β -Pyrrolic and Bridging Positions. *Chem. Eur. J.* 2017, 23, 14786–14796.
- (39) Zatsikha, Y. V.; Didukh, N. O.; Swedin, R. K.; Yakubovskyi, V. P.; Blesener, T. S.; Healy, A. T.; Herbert, D. E.; Blank, D. A.; Nemykin, V. N.; Kovtun, Y. P. Preparation of Viscosity-Sensitive Isoxazoline/Isoxazolyl-Based Molecular Rotors and Directly Linked BODIPY—Fulleroisoxazoline from the Stable *meso-*(Nitrile Oxide)-Substituted BODIPY. *Org. Lett.* **2019**, *21*, 5713—5718.
- (40) Swedin, R. K.; Zatsikha, Y. V.; Healy, A. T.; Didukh, N. O.; Blesener, T. S.; Fathi-Rasekh, M.; Wang, T.; King, A. J.; Nemykin, V. N.; Blank, D. A. Rapid Excited-State Deactivation of BODIPY Derivatives by a Boron-Bound Catechol. *J. Phys. Chem. Lett.* **2019**, *10*, 1828–1832.
- (41) (a) Becke, A. D. Becke's three parameter hybrid method using the LYP correlation functional. *J. Chem. Phys.* **1993**, *98*, 5648–5652. (b) Lee, C.; Yang, W.; Parr, R. G. Development of the Colle-Salvetti correlation-energy formula into a functional of the electron density. *Phys. Rev., B* **1988**, *37*, 785–789.
- (42) Tomasi, J.; Mennucci, B.; Cammi, R. Quantum mechanical continuum solvation models. *Chem. Rev.* **2005**, *105*, 2999–3093.
- (43) Wachters, A. J. H. Gaussian Basis Set for Molecular Wavefunctions Containing Third-Row Atoms. *J. Chem. Phys.* **1970**, 52, 1033–1036.
- (44) McLean, A. D.; Chandler, G. S. Contracted Gaussian basis sets for molecular calculations. I. Second row atoms, Z = 11-18. *J. Chem. Phys.* **1980**, 72, 5639–5648.
- (45) Frisch, M. J.; Trucks, G. W.; Schlegel, H. B.; Scuseria, G. E. et al. *Gaussian 09*, Revision D.1, Gaussian, Inc.: Wallingford, CT, 2009. See Supporting Information for full citation.
- (46) Tenderholt, A. L. QMForge, Version 2.1. Stanford University, Stanford, CA.